Quantum Electronics **48** (2) 105–114 (2018)

INVITED PAPER

https://doi.org/10.1070/QEL16540

Thin-film X-ray filters on microstructured substrates and their thermophysical properties

A.V. Mitrofanov

Abstract. **It is shown that structured substrates having micron- or submicron-sized through holes and coated with an ultrathin organic film can be used for the fabrication of thin-film X-ray filters via direct growth of functional layers on a substrate by sputter deposition, without additional complex processing steps. An optimised process is considered for the fabrication of X-ray filters on support structures in the form of electroplated fine nickel grids and on track-etched polymer membranes with micron- and submicron-diameter through pores. 'Optimisation' is here taken to mean matching the sputter deposition conditions with the properties of substrates so as to avoid overheating. The filters in question are intended for both imaging and single-channel detectors operating in the soft X-ray and vacuum UV spectral regions, at wavelengths from 10 to 60 nm. Thermal calculations are presented for the heating of ultrathin layers of organic films and thin-film support substrates during the sputter deposition of aluminium or other functional materials. The paper discusses approaches for cooling thin-film composites during the sputter deposition process and the service of the filters in experiments and gives a brief overview of the works that utilised filters produced by the described technique on microstructured substrates, including orbital solar X-ray research in the framework of the CORONAS programme and laboratory laser plasma experiments.**

Keywords: *thin-film X-ray filters, microstructured substrate, thermophysical properties.*

1. Introduction

More than a quarter century ago, researchers at the P.N. Lebedev Physical Institute (LPI), Russian Academy of Sciences (RAS), began work aimed at creating a then-new class of X-ray telescopes and spectral coronagraphs for studies of the Sun's corona in the soft X-ray and vacuum ultraviolet spectral regions [1]. The innovation was that normal-incidence focusing multilayer X-ray mirrors designed and fabricated by researchers at the Institute for Physics of Microstructures, RAS, in cooperation with their colleagues at LPI were used for the first time as key optical components of instruments. As a result of that work, a new generation of telescopes were fabricated, tested and then placed in a low Earth orbit: TEREK telescope, with 17.5- and 30.4-nm channels (Phobos-1 project, 1988) [2]; TEREK-K telescope for the CORONAS-I satellite (1994), with 13.2-, 17.5- and 30.4-nm channels; and finally SRT-C assembly of the SPIRIT instrumentation for the CORONAS-F satellite (2001–2005), with two multichannel telescopes having transmission bands at wavelengths of 17.1, 19.2, 28.4 and 30.4 (telescope T1) or 17.5 and 30.4 nm (telescope T2) [3, 4]. Note that, between 1988 and 2009, ten space vehicles carrying telescopes and spectrometers for studies of the Sun in the soft X-ray spectral region were launched into Earth's orbit, including four multichannel instrument systems with six X-ray telescopes made at LPI. The detectors used in those instruments were various types of windowless position-sensitive microchannel plate (MCP) detectors, X-ray luminescence converters produced on cylindrical and tapered fibre-optic waveguides (focusing cones) and CCD detectors. To protect the detectors from undesirable solar background radiation in the long-wavelength part of the spectrum, researchers at LPI in cooperation with their colleagues at the Laboratory of Nuclear reactions, Joint Institute for Nuclear Research (Dubna), designed and fabricated universally applicable (suitable for all types of detectors used at the time), interchangeable, replaceable thin-film X-ray filters on microstructured substrates, intended for application in the soft X-ray and vacuum UV spectral regions for operation with imaging optics. This paper addresses primarily the thermophysical (thermal) properties of filters on fine-structured substrates.

A.V. Mitrofanov P.N. Lebedev Physical Institute, Russian Academy of Sciences, Leninsky prosp. 53, 119991 Moscow, Russia;
e-mail: mitrofa@sci.lebedev.ru

Received 18 October 2017; revision received 27 November 2017
Kvantovaya Elektronika **48** (2) 105–114 (2018)
Translated by by O.M. Tsarev

2. Filters in X-ray astronomy of the Sun

Essentially all the types of ultrasoft X-ray and extreme ultraviolet (XUV) detectors used in X-ray astronomy instruments and laboratory plasma diagnostics, including so-called solar-blind photodetectors, are to some extent sensitive to background radiation in a wide wavelength range (from the UV to near-IR spectral region, with a boundary near 1.1 μm in the case of a CCD silicon array detector or single-channel silicon photodiode with no protective filter). The Sun and many laboratory plasma objects emit in the operating spectral region much less in comparison with the long-wavelength background (difference in energy flux by several orders of magnitude). Because of this, in solar X-ray astronomy and ground-based experiments, use is made of protective filters, which intercept background radiation and have a transmission band in the soft X-ray or vacuum UV spectral region.

Solar telescopes and radiometers intended for application in these spectral regions typically employ systems of two or three separate thin-film filters whose transmission spectrum is matched to characteristics of the detector and optical components of the instrument (reflective mirrors and reflective or

transmissive gratings). The filters should meet stringent requirements in terms of a variety of parameters. They should be robust, durable structures transparent in the operating spectral region, capable of effectively intercepting background radiation (often at a level of above seven orders of magnitude), free of perforation and other hidden or through defects (pinholes) [5–8] and capable of withstanding high mechanical, acoustic and thermal loads, meeting climatic requirements for testing and storage of filters, possessing an acceptable radiation resistance and withstanding the air pressure difference arising in the instrument when the telescope is launched into Earth's orbit. This refers primarily to large-aperture front filters, which are placed on support structures in front of the mirror objective of X-ray telescopes. A filter that is mounted in front of a detector or produced by sputter deposition directly on its entrance surface (e.g. on the sensitive surface of a CCD array detector) is referred to as the detector filter [5, 6]. Its dimensions are far smaller than those of large front filters, but it also should meet stringent requirements as to the limiting mechanical loads, stability of its characteristics (durability), uniformity, absence of pinholes and the ability to withstand the thermomechanical stress arising during the fabrication process and experiments. It is such filters that are addressed in this paper. Reviews of other researchers' work in this area, concerned with the fabrication and operation of thin-film filters in space X-ray optics, can be found in Refs [5–15].

It is worth noting that, in the spectral range under consideration (soft X-rays and vacuum UV with wavelengths from 10 to 60 nm), the main radiation absorption mechanism is the photoelectric effect, and it is in this range that uniform films of any materials have extremely large absorption coefficients (10^{-6} to 10^{-5} cm^{-1}). For this reason, in contrast to the classic (hard) X-ray region (wavelengths of ~0.1 nm), where massive films and thick windows and foils are employed as filters and windows, here use is made of extremely thin samples in the form of single layers or multilayers. When radiation passes through such systems and optical elements based on them, they change the spectral composition of the beam, but the main goal of filters in X-ray astronomy is to intercept radiation beyond the operating range of the instrument. This work deals primarily with absorbing filters, but its results are applicable as well to diffraction X-ray filters and reflection filters. The mechanism of long-wavelength background suppression by thin-film filters is determined by a joint contribution of absorption, surface reflection and, occasionally, scattering effects.

3. Detector filter design

A detector filter can be interchangeable (replaceable) or form a single structure with the detector [5, 6]. The choice of the type of filter is determined by experimental conditions, detector design, properties of the emitting object, those of the medium where measurements are performed, etc. In the case of silicon imaging detectors and photodiodes, wavelength-selective single-layer or, more frequently, submicron-thick multilayer films produced on the active area of the detector are used as protective filters integrated with the photodetector [5, 6]. The use of a multilayer structure is necessary for selecting a preset (operating) passband of the filter, improving the service performance of the filter owing to the compensation for the mechanical stress in the layers and the absence of a crystallisation threshold of thin amorphous layers and protecting the internal elements of the filter by an ultrathin barrier film.

Despite the obvious advantages of a filter–photodetector combination as a single functional component, in many cases it is more convenient to use a replaceable protective filter which can be mounted in front of the detector or replaced for a variety of reasons. The design of a detector with a replaceable filter allows one to replace the filter by a new one before placing the telescope in an orbit and to change to another spectral range of measurements and is convenient for ground-based preflight calibrations of apparatus. Moreover, if a commercially available windowless microchannel plate multiplier with open channels is used as a detector of an instrument, it is problematic to produce a filter integrated with it on the input MCP surface. X-ray imaging detectors, including windowless MCP brightness amplifiers, are expensive and delicate instruments. Because of this, additional processing steps on the sensitive surface of a photodetector may influence its performance in fabricating a protective filter integrated with the detector [16]. The problem does not arise if a replaceable protective detector filter is used in an instrument.

Consider specific features in designing and fabricating a replaceable filter for ultrasoft X-ray and XUV detectors: imaging detectors or single-channel photodiodes. The filter should consist of a metallic layer, e.g. aluminium 0.1–0.2 μm in thickness, or a multilayer thin-film structure transparent in the operating range and capable of intercepting background radiation (at a level of several orders of magnitude in terms of energy flux) in the long-wavelength part of the spectrum, starting at $\lambda \geqslant 0.1$ μm. Since the total thickness of a thin-film structure does not exceed a few tenths of a micron, at a detector window area in the range 1–10 cm^2 the free-standing film of the filter should be reinforced by some sufficiently rigid support structure, e.g. by a highly transparent grid with an optimal period, which is chosen based on experimental conditions and the geometry of the sensitive detector cells. Note that, under laboratory conditions and in experimental X-ray lithography schemes in some cases one can use thin-film designs without rigid support structures.

A standard process for the fabrication of a replaceable thin-film filter includes sputter deposition of a filter structure on a flat, smooth substrate (as a rule, with the use of a temporary, 'sacrificial' layer), separation of the filter from the substrate and securing to a transparent support structure, followed by the removal of the sacrificial coating. Basically, it is a version of the replica method and the X-ray filter itself is a uniform large-area, thin-film, defect-free replica taken from a smooth surface of a heatsink substrate and used as an X-ray window of a detector. The detector filter fabrication process can be significantly simplified by excluding the replication of the sputter-deposited filter structure, a rather complex step. However, direct sputter deposition of filter layers on a free-standing thin film or a sacrificial polymer layer without effective heat dissipation leads to thermal breakdown of the filter under essentially any sputter deposition conditions (in all sputtering systems) because of the low heat capacity of the thin layer, the poor thermal conductivity of polymers and the absence of effective heat dissipation from a heated sample.

This seemingly insurmountable obstacle can be obviated by securing an ultrathin film or sacrificial polymer layer of the filter on a fine-structured substrate with micron- or submicron-sized open through windows before deposition. As such substrates, we used track-etched membranes (polymer films with micron-diameter through pores) and flat thin nickel

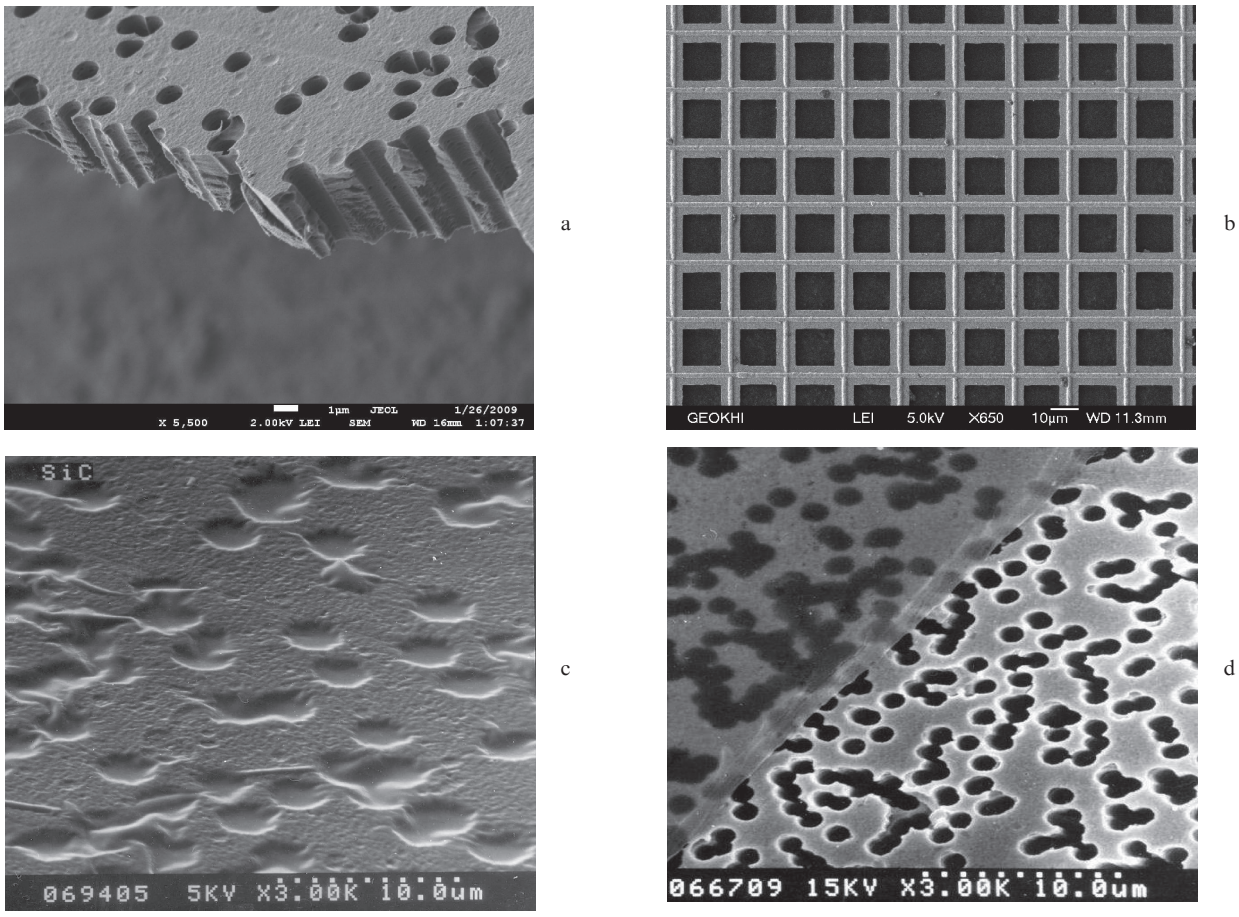

Figure 1. Electron micrographs of (a) a fracture surface of a track-etched membrane, (b) a supporting nickel microgrid, (c) the surface of a filter in the form of a silicon carbide film on a track-etched membrane and (d) a portion of the surface of a thin-film coating (0.1-µm-thick nickel film) on a porous membrane.

microgrids, to which ultrathin (40 to 60 nm) polyvinyl formal (formvar) films were tightly attached (glued). One function of the grids and membranes was to dissipate the heat released during the deposition process as a result of the condensation of metal (or insulator) vapour on the ultrathin formvar film. This is the main distinction of our method from the standard thin-film filter fabrication procedure, in which layers are first sputter-deposited on a bulk heatsink substrate, following which the layer or multilayer structure is separated from the substrate and the layers of the filter are secured to a supporting grid.

Using the proposed method, we fabricated series of interchangeable submicron-thick metallic and (multilayer) composite (metal–polymer and metal–ceramic) filters from Al, Mo, Si, Ni, Rh, Nb, SiC and some other materials on grids and porous substrates with cylindrical through pores at a normal orientation of their axes with respect to the filter surface. The thickness of the support membranes varied from filter to filter (5–23 µm), whereas the pore diameter in the membranes was roughly the same (0.5–3.2 µm). The thickness of the regular nickel grids, with a structure period of 20, 16 or 10 µm, was about 3 µm. An important component of a filter on a fine-structured substrate is its frame, which is used as a filter holder, light 'lock', antivibration (damping) element and conductor for effective heat dissipation from the heated filter to a colder base of a telescope or benchtop spectroscopic instrument. Figure 1 shows some of the fine-structured support substrates used by us, and portions of the surface of membranes with sputter-deposited metallic layers. (Samples were prepared and electron micrographs taken by O. Orelovich, A. Rusakova, A. Burmistrov and T. Gromova.)

4. Solving the heat problem

Consider now in greater detail the heating of and heat dissipation from a free-standing uniform thin polymer film of thickness δ when a substance, e.g. aluminium, is sputter-deposited on its surface. Let the film have no substrate, be in vacuum and be secured to (stretched onto) a circular frame or specimen disc of diameter $d = 2R$ with good thermal contact along its perimeter. The temperature of the frame, T_1, is maintained constant and in general may differ markedly from room temperature, T_0. Let $Q_c = m_t\omega$ be the density of a uniform heat flux on the surface of the film due to metal vapour condensation on the sample. Here $m_t = \rho^*\delta_t^*$ is the mass deposition rate of the substance on the substrate (which is taken to be constant in our estimates); ω is the total energy per unit mass released during the condensation of the substance on the substrate; ρ^* is the density of the deposit (which for simplicity is taken to be independent of the thickness of the layer); and δ_t^* is the growth rate of the deposit. The heating of the sample by the thermal radiation from the metal vapour source and the heating by rarefied gas at a low pressure in the sputter chamber are here left out of consideration. In the case of thermal

evaporation, ω is roughly equal to the density of the atomisation enthalpy of the substance [17]:

$$\omega = c_1\Delta T_1 + L + c_2\Delta T_2 + q, \quad (1)$$

where c_1 and c_2 are the specific heats of the metal in solid and liquid phases, respectively; ΔT_1 is the difference between its melting point and the condensation (substrate) temperature; ΔT_2 is the difference between the evaporation temperature and melting point; and L and q are the specific heats of melting and vaporisation. For example, the ω of Al evaluated by formula (1) is about 15 MJ kg^{-1}, or 40 GJ m^{-3} [17], i.e. 4.1 eV per atom. If aluminium is deposited on a film in an rf gas discharge (magnetron sputtering), rather than from a resistively heated tungsten boat or heated ceramic crucible, atoms arriving at the sample are 'hotter' than those in the case of thermal evaporation, because they have an extra kinetic energy of $\sim$1 eV per atom. Therefore, the thermal load on the substrate will be noticeably higher than that in the case of thermal evaporation [formula (1)] at the same deposition rate δ_t^*.

In thin-film X-ray filters intended for the soft X-ray or vacuum UV spectral region, the thickness of their metal layer, δ^*, or the total thickness of their functional layers (in the case of a multilayer structure) is of the order of tens or hundreds of nanometres, depending on their intended application, and the deposition rate δ_t^* during filter fabrication may exceed 100 nm s^{-1} [8]. The heat flux density on the substrate during Al sputter deposition is then a factor of 2.5–3 higher than the so-called solar constant, α = 1370 W m^{-2}. In filters intended for experiments in the soft X-ray region, an acceptable polymer layer is usually thinner than the functional metal layer: $\delta \leqslant \delta^*$. Because of this, it is convenient to use ultrathin polymer layers as substrates. They should be very thin (no more than a few tens of nanometres in thickness) or should be removed after the filter fabrication process by some technique, e.g. by photoetching [9].

Consider the case where the deposition rate (and the thermal load ω) are low and the temperature of the thin-film substrate is substantially lower than the thermal breakdown threshold. In the very first instance of sputter deposition, when the thickness of the deposit, δ^*, is far smaller than that of the substrate, δ, the thermal resistance of the former is high, heat is dissipated to the boundary of the sample due to heat conduction in the polymer film and the quasi-equilibrium (steady-state or slowly varying) radial temperature profile in the sample can be described by the approximate formula

$$T(r) = T_1 + \rho^*\delta_t^*\omega\,(R^2 - r^2)/(4\lambda\delta). \quad (2)$$

Here λ is the thermal conductivity of the polymer (a weak function of T at temperatures of the order of 300 K [18]) and r is the distance from the centre of the sample to the point under consideration. This is an approximate relation obtained by solving a steady-state nonhomogeneous heat (energy balance) equation for the problem with a heat source and a fixed temperature on the boundary contour. Note the obvious fact that the spatial temperature profile (2) in this problem has the same form to within a dimensional constant as that in a long electric wire carrying a direct current with ohmic losses at a constant temperature on the wire surface if the heat dissipation mechanism in the wire is conventional heat conduction (see Ref. [19], p. 106, problem 670). The solution to (2) for a formvar film ignores the heat loss due to radiative cooling, because the film is taken to be optically thin and completely transparent to thermal radiation. The sample experiences the maximum overheating ΔT in the centre of the ring (r = 0):

$$\Delta T_{max} = T_{max} - T_1 = \rho^*\delta_t^*\omega d^2/(16\lambda\delta). \quad (3)$$

Figure 2 shows heating isotherms (thermal load against the diameter of the sample on the mount, $d = 2R$), $\Delta T = \Delta T_{max}$ = const, for a 60-nm-thick formvar film used in our experiments (Fig. 2). If the sample has a small size, the problem can be treated as steady-state: according to (2), the characteristic setting time of the temperature profile on the surface of the sample, $\tau_1 \cong R^2\rho C_p/(4\lambda)$, is shorter than the time (τ_2) it takes to heat the film to the point where the high deposition rate leads to the thermal destruction (disintegration) of the polymer film. In this case, we have $\tau_2 \geqslant C_p\rho\delta\Delta T_{crit}/(\omega\rho^*\delta_t^*) \geqslant \tau_1$. The ΔT_{crit} of formvar slightly exceeds 100 °C. Owing to the heat dissipation across the interface, the actual time exceeds this estimated 'lifetime' of the film. The temporal temperature profile of the sample at different points with a radius r can be more accurately described by the formula

$$T(r,t) = T_1 + \rho^*\delta_t^*\omega(R^2 - r^2)[1 - \exp(-t/\tau_0)]/(4\lambda\delta). \quad (4)$$

Here the time constant $\tau_0(r)$ for the evolution of the temperature profile of the sample during the sputter deposition process depends on the radial coordinate in the film:

$$\tau_0(r) = (R^2 - r^2)\rho C_p/(4\lambda). \quad (5)$$

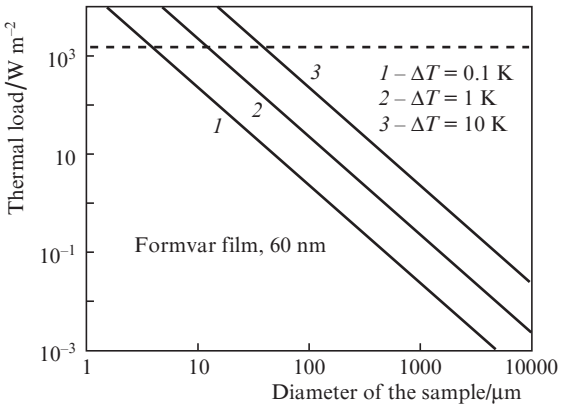

Figure 2. Thermal load against the diameter of the sample, d, for deposition on a free-standing formvar film secured to a cooled mount, at a given overheating ΔT in the centre of the film. The thickness of the formvar film is 60 nm. Here and in Figs 3 and 7, the dashed line indicates the level corresponding to the solar constant in a low Earth orbit.

Relation (4) is analogous to the known formula for the temperature profile of a free-standing thin polymer substrate on a standard copper ring (3-mm specimen disc) when an object is placed in a holder of an electron microscope operating in probe defocusing mode [20]. In roughly estimating the time it takes for a steady-state solution to be reached, the heat capacity and thermal conductivity of formvar and other polymers can be taken to be constant, temperature-independent quantities. Numerical values of thermal constants of some materials used in the fabrication of thin-film X-ray filters and support structures are listed in Table 1 for the temperature range

Table 1. Reference values of thermal characteristics of some materials used in the growth of thin-film layers and fabrication of support structures for securing the films and dissipating heat in X-ray filters*.

Material	Density $\rho/10^3$ kg m^{-3}	Specific heat C_p/J kg^{-1} K^{-1}	Thermal conductivity λ/W m^{-1} K^{-1}	Linear expansion coefficient/10^{-6} K^{-1}
Formvar	1.23	2000	0.24	–
PET	1.39	1300	0.14	20–80
Polyimide	1.43	1090	0.10–0.35	28**
Aluminium	2.7	900	230	23.5
Copper	8.96	390	400	17
Nickel	8.9	450	90	13
Molybdenum	10.2	250	138	5
Zirconium	6.49	280	23	5.9
Rhodium	12.4	240	150	8.5

*http://www.goodfellow.com/catalogue/GFCatalogue.php?Language=E.
**Data for UPILEX-R polyimide film (UBE Industries Ltd, Japan), an analogue of the Kapton H polymer material (DuPont).

300–400 K. These data are borrowed from http://www.goodfellow.com/.

The dashed line in Fig. 2 indicates the level of the 'solar' constant (in Earth orbit). This level is known to roughly correspond to the heat flux incident on a cooled substrate in the case of aluminium deposition via 'explosive' thermal evaporation which was used previously in the fabrication of large high-quality thin-film X-ray filters for the Apollo Telescope Mount [8].

To compare the estimated heating of a thin formvar film with real data for different sputter-deposition conditions, we present the heat release on a substrate as a function of aluminium deposition rate for the thermal evaporation of the metal (Fig. 3) with no allowance for the fraction of the heat flux on the substrate from the heater (tungsten boat). In the fabrication of thin-film X-ray filters, metals, including aluminium, were sputter-deposited at a rate $\delta_t^* \approx 0.1-0.3$ nm s^{-1} in the case of rf magnetron sputtering and $\delta_t^* \approx 5-10$ nm s^{-1} for aluminium deposition in vacuum via thermal evaporation. Under the sputter-deposition conditions chosen, the thermal load on the formvar film was 10–1000 W m^{-2} (Fig. 3).

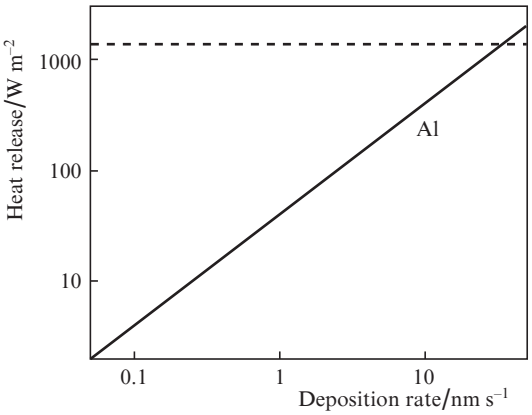

Figure 3. Heat release due to aluminium vapour condensation on a formvar film as a function of Al deposition rate.

It follows from the above estimates and the data in Figs 2 and 3 that direct sputter deposition of a substance on thin and ultrathin free-standing organic films can be performed without overheating the sample, let alone without thermal breakdown, if the pore diameter or characteristic cell size in the support structure is reduced down to the micron range and, simultaneously, effective heat dissipation from the support structure is ensured in order to avoid its overheating over the entire working surface of the filter (to the threshold operating temperature of the functional layers of the filter).

Consider now possible approaches to heat dissipation from the microstructured substrate to which a film is secured with thermal contact. Under vacuum or at a low pressure, the sample can be cooled during the deposition process either via radiative heat dissipation from the support structure or due to heat conduction driven by the temperature gradient arising when the substrate with a deposit or a specimen disc is placed on a cold thermostated or cooled heat-dissipating flange. In some designs, the contribution of radiative cooling can be comparable to that of heat conduction.

In our work, we used both approaches for heat dissipation from the thin film during filter fabrication by sputter deposition. As a thermal radiator and support structures, we used polyethylene terephthalate (PET) polymer track-etched membranes [21] ranging in thickness from 5 to 23 μm (in different samples) and having through (open) pores uniform in diameter (0.5–3.2 μm). The pores in the membranes were nearly cylindrical or in the shape of a sandglass with a small taper. We used both parallel orientation of the pore axes (along the normal to the sample surface) and membranes with oblique pores. The pores in the film ensured transport of X-rays or vacuum UV radiation in the operating range, and the polymer matrix, a 'skeleton' of the filter, acted as a thermal radiator in the filter fabrication step and when the filter operated under experimental conditions. Some polymers, such as polyethylene terephthalate, polyethylene naphthalate, polycarbonate, polyimides and others, have strong absorption bands in the mid-IR spectral region, between 5 and 15 μm [22]. Films of such materials 10–20 μm or more in thickness are good absorbers of thermal radiation from bodies heated to several tens of degrees Celsius above room temperature and, accordingly, effectively dissipate heat through emission (Fig. 4). It is this type of radiative cooling, with the use of polymer films metallised on one side, which is used in space engineering in passive thermal control systems [23]. In such a case, the uncoated polymer surface serves as the outer radiator surface, and the metallised side faces the casing of the object being cooled.

Figure 5 shows the transmission spectrum of a 23-μm-thick Hostaphan PET film (Mitsubishi Polyester Films) in the wavelength range 2–16 μm. (The measurements were made

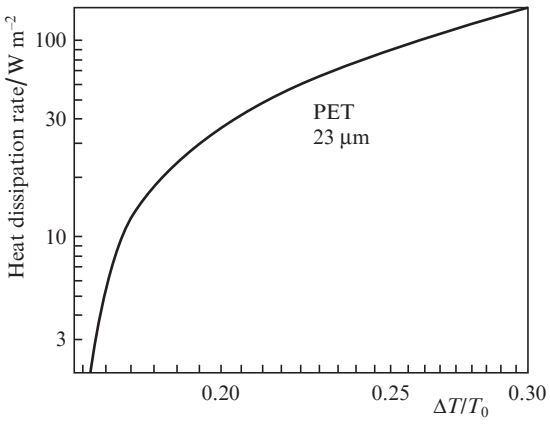

Figure 4. Rate of radiative heat dissipation on one side of a 23-μm-thick PET film vs. overheating of the film relative to the ambient medium.

by O. Kristavchuk at room temperature on a Nicolet 6700 Fourier transform IR spectrometer.) The overall composition of PET is $C_{10}H_8O_4$ and its structural formula is

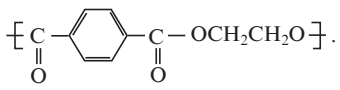

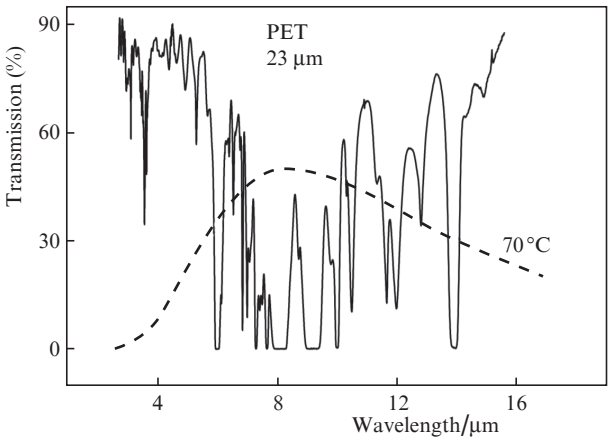

Figure 5. Transmission spectrum of a 23-μm-thick PET film in the mid-IR spectral region. The dashed line represents the 70 °C black-body radiation spectrum in arbitrary units.

In the spectral range under consideration, the aromatics in PET have a large number of absorption peaks [22]. In particular, the stretching –C=C– mode is represented by two peaks: at 1578 cm^{-1} (6.34 μm) and 1505 cm^{-1} (6.64 μm). The ester compound has strong bands in its absorption spectrum. The C=O carbonyl group shows up as a strong peak at 1726 cm^{-1} (5.79 μm). Ester compounds also have strong absorption bands and peaks in the mid-IR spectral region. Those in the spectrum of PET (Fig. 5) correspond to the stretching –C–O, C–C(O)–O and O–C–C modes at 1264 cm^{-1} (strong absorption band centred at 7.91 μm) and 1103 cm^{-1} (strong peak at a wavelength of 9.07 μm) for the former and latter compounds, respectively. The strong band at a wavenumber of 729 cm^{-1} (13.7 μm) corresponds to bending vibrations of the $-CH_2-CH_2-$ part of the polymer molecule backbone. The above peaks and bands are located near the maximum in the black-body radiation spectrum several kelvins above room temperature (Figs 5, 6). Therefore, a relatively thick PET film can serve as a good radiator for effective heat dissipation from film structures during the sputter deposition process.

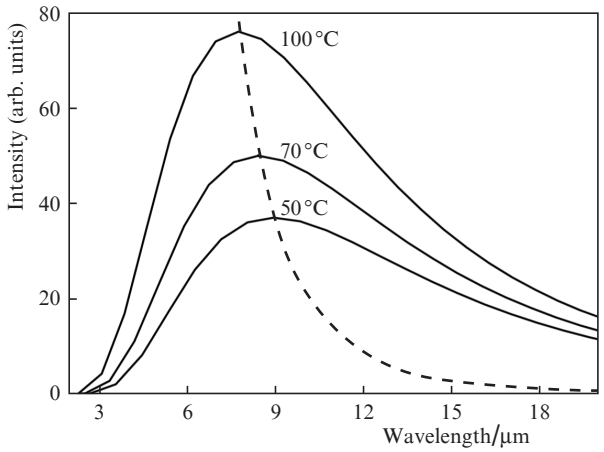

Figure 6. Black-body radiation spectra at different temperatures.

From the data presented in Fig. 5, we can find the spectral emissivity $\varepsilon_\lambda(T)$ of a partially transparent polymer film [24, 25] and evaluate its total emissivity by the well-known formula

$$\varepsilon(T) = \frac{\int \varepsilon_\lambda(T)\, U_\lambda(T)\, \mathrm{d}\lambda}{\int U_\lambda(T)\, \mathrm{d}\lambda}, \qquad (6)$$

where $U_\lambda(T)$ is the monochromatic black-body radiation intensity calculated by Planck's formula [24]. In the transmission spectrum $\tau(\lambda)$ of a 23-μm-thick PET film (Fig. 5) heated to 70 °C, the total emissivity $\varepsilon(T)$ of the film in the range 3–16 μm was determined to be about 0.6. This temperature approximately corresponded to a real heating of a polymer substrate during aluminium sputter deposition in a Sputron-2 system (Balzers). It is seen in Fig. 6 that, when a sample is heated from room temperature to 100 °C (near the limiting operating temperature of a formvar film on a substrate in the form of a porous PET membrane), the $U_\lambda(T)$ spectral characteristic of black-body radiation varies in accordance with Planck's formula. This leads to a nonmotonic variation in $\varepsilon(T)$ within a few percent, as shown previously for PET [26]. At the same time, according to measurement results reported by Adamov and Savinich [26], the response of $\varepsilon(T)$ to the slight broadening of the absorption bands of the polymer with increasing temperature in the temperature range in question is insignificant compared to the temperature variation of the function $U_\lambda(T)$. Note that room-temperature transmission spectra of PET films with other thicknesses (6 and 25 μm) can be found in Sala [25].

Even though the 23-μm-thick PET film is partially transparent to IR radiation (Fig. 5), it effectively dissipates heat in vacuum if heated to several tens of degrees Celsius above room temperature T_0, at which the casing and ambient atmosphere of the sputtering apparatus are maintained. Figure 4

shows the calculated rate of radiative heat dissipation on one side of a 23-μm-thick PET film vs. overheating of the film relative to the temperature of the ambient medium. For these estimates, the total emissivity of the film was taken to be equal to the measured one ($\varepsilon = 0.6$) and the film was assumed to be continuous and homogeneous. Together with the data in Fig. 3, this curve allows one to estimate the limiting metallisation rate of an ultrathin polymer film on a porous PET substrate when heat dissipation is only due to radiative heat transfer. In the case of aluminium sputter deposition on a formvar film, this rate is about 10 nm s^{-1} (the corresponding thermal load is slightly less than 100 W m^{-2}).

5. Role of the thermal conductivity of the support structure and deposit

Let us estimate the contribution of heat conduction to the cooling of a fine-structured substrate due to the temperature gradient arising during sputter deposition. At the beginning of the deposition process, when the thickness of the metallic deposit is small, the thermal conductivity of the sample is determined by the substrate material with allowance for the effect of porosity, which reduces the thermal conductivity of the porous substrate by about a factor of $1 - P$ relative to a homogeneous one, where P is the effective porosity of the fine-structured support structure. This approximation is justified if the grid opening size or the pore diameter in a track-etched membrane is much smaller than the diameter of the sample, which is almost always satisfied. If the transmission of a fine-structured substrate is not very high, its porosity can be left out of account in roughly estimating its temperature profile, and the sample can be treated as homogeneous. The steady-state (quasi-equilibrium) temperature profile of the support structure can then be found using (2) and the maximum temperature can be evaluated using (3) with allowance for the geometry and thermal characteristics of the film–substrate system. Recall that the peripheral part of the substrate is in close contact with a cold flange (thermostated at temperature T_1).

The similarity criterion in terms of the size parameter $d^2/(\lambda\delta)$ at a given sputter deposition rate allows one to easily obtain the temperature profile and maximum overheating of a sample from characteristics of its support substrate and the data in Fig. 2. In particular, Fig. 7 shows overheating vs. sample diameter isotherms calculated for a 23-μm-thick PET film at different thermal loads with no allowance for radiative cooling. The data presented in Figs 2 and 7 were used in choosing a moderate operation mode of the sputter deposition apparatus for metallising a homogeneous polymer film on a grid or porous track-etched membranes serving as fine-structured substrates for thin-film X-ray filters of solar telescopes or independent diffraction filters of single-channel radiometers.

When the thickness of the metallic layer, δ^*, on the polymer film, of thickness δ, reaches a certain level, sputter deposition leads to a marked increase in the thermal conductivity of the sample. Since thermal equilibrium across the deposit sets in almost instantaneously (compared to other characteristic time constants of the sputter deposition process), it is easy to show that the effective thermal conductivity of a bilayer film (with no allowance for properties of the interface) is

$$\lambda_{\text{eff}} = (\lambda^*\delta^* + \lambda\delta)/(\delta^* + \delta) = (\lambda + \lambda^* x)/(1 + x), \qquad (7)$$

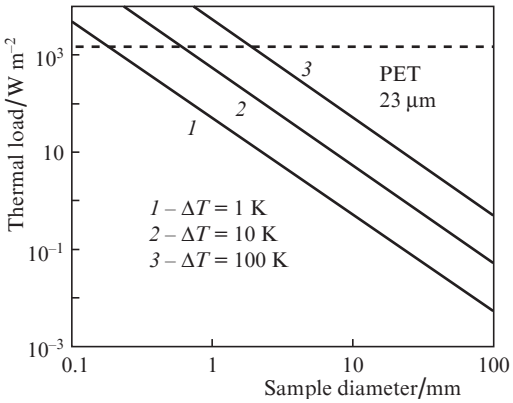

Figure 7. Uniform (homogeneous) thermal load as a function of sample diameter d for a 23-μm-thick PET film secured on a cooled mount, at the specified overheating ΔT in the centre of the film.

where $x = \delta^*/\delta$ is the ratio of the thickness of the metallic layer to that of the polymer film. Relation (7), valid for a bilayer sample, can be extended, with some limitations, to a multilayer with a given configuration and characteristics of the layers. The use of λ_{eff} is convenient in calculating the thermal regime of a sample during the growth of filter layers on a fine-structured substrate by sputter deposition or in measurements with a filter placed in front of a detector in an experimental setup with a high-power radiation source.

Figure 8 shows calculated $\lambda_{\text{eff}}(x)$ curves for an aluminium–PET composite layer, aluminised ultrathin formvar film and thin-film rhodium coating on a thin homogeneous intermediate formvar layer of a nickel microgrid, a thermal analogue of a 3-μm-thick fine-structured electroplated nickel grid with a 10-μm period and 53% transmission [27, 28]. Note that, if the thickness of the metallic layer grown on a thin-film substrate is under 10–20 nm, rigorous calculations should use experimental data rather than reference data on the thermal conductivity of bulk materials. Due to size effects, the role of the interface and, in a number of cases, a nonuniform (island) structure of very thin deposits (which is typical of thermal evaporation), the thermal conductivity of ultrathin single layers and multilayer films differs from that of bulk materials.

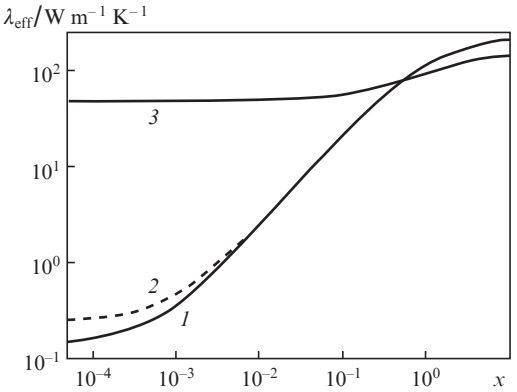

Figure 8. Effective thermal conductivity of a bilayer film as a function of the ratio of the thickness of the coating to that of the thin-film substrate, x, for an (*1*) aluminised PET film, (*2*) aluminised ultrathin formvar film and (*3*) rhodium film grown by sputter deposition on a formvar layer and thin nickel foil substrate.

The issue of the effective thermal conductivity of multilayer X-ray filters has been little studied and requires further investigation according to a number of researchers [29]. Note that, in the case of the curves in Fig. 8, there are also limitations on the maximum x-coordinate. The reason for this is that the metallic deposit should not be too thick for a variety of reasons, of which the most important are the strength of the filter and its transmission in the operating spectral range. Usually, in the case of an ultrathin formvar substrate (a few tens of nanometres in thickness, Fig. 1) for aluminium filters, it is reasonable to estimate the effective thermal conductivity at x values in the range $0.3 \leqslant x \leqslant 3$. In the case of the metallisation of 0.23-μm-thick track-etched PET membranes (Fig. 8), the above approximate formulas and curves are meaningful in the range $0.001 \leqslant x \leqslant 0.01$.

To metallise membranes, we used not only aluminium but also other metals, including nickel, molybdenum and titanium.

6. Experimental work in which X-ray filters on fine-structured substrates were used

Fine-structured substrates for detector filters were first used in the TEREK experiment on board the Phobos-1 spacecraft [2].

In the MX ultrasoft X-ray channel (operating wavelengths of 17.5 and 30.4 nm), a thin (150 nm) aluminium film on a nickel grid with a 20-μm period was placed in front of a luminescent converter. In an equipment spare package, a metallised track-etched membrane was used instead of this filter, and an aluminium film of the same thickness was produced on its outer surface (facing the detector). The thickness of the membrane was 17 μm, the pore diameter in it was 2.8 μm, and the pore density was $N = 4\times10^6$ cm^{-2}. Subsequently, we used this type of membrane, with a pore diameter increased to 3.2 μm, in the TEREK-K solar telescope [30].

In this stage in the development of new apparatus, attention focused on issues pertaining to the fabrication of high-quality aluminium layers, ways of securing them to fine-structured substrates and the testing of the physical properties of the X-ray filters. Layers of aluminium films were produced by a standard procedure: vacuum sputter deposition on cooled smooth glass substrates. The layer was then separated from the substrate and transferred to a support structure. Thermal evaporation was carried out in an Alcatel SCM-451 cryogenically pumped high-vacuum deposition system [31].

A different sputter-deposition system [31] enabled the first direct sputter deposition of nickel and other metals on free-standing ultrathin organic substrates, which were secured in close contact on track-etched membranes with through pores. Later, this approach was used in the fabrication of a very complex thin-film filter for the TEREK-K telescope [30], whose key component was a free-standing silicon carbide film [32]. The point is that, in one of the channels of this telescope, the same detector (sequentially) detected radiation at wavelengths of 13.2, 17.5 and 30.4 nm. The combination of requirements for the transmission of the filter at these spectral lines and the blocking of the strong solar line at a wavelength of 121.7 nm (H L_α), as well as the absorption edges and the limited range of suitable materials, determined the final configuration of the filter [30, 32]. In the flight version, the detector filter in the MX channel consisted of a 30-nm-thick silicon carbide film, 5-nm-thick molybdenum layers and a 35-nm-thick slightly oxidised aluminium layer. The layers of the filter were secured on the surface of a metallised track-etched membrane containing about 3-μm-diameter through pores. The sacrificial formvar layer underlying the silicon carbide film was fully removed in the pore channel region by room-temperature photoetching in air. In addition to this filter, an aluminium–formvar composite on a track-etched membrane was placed in close contact in front of the X-ray imaging detector in the HR channel (17.5 nm) [30].

Further progress in designing thin-film filters on fine-structured substrates was made by improving the spatial resolution of the X-ray telescopes in the SRT-C assembly of the SPIRIT instrumentation for the CORONAS-F satellite (2001–2005). It had two telescopes with transmission bands at wavelengths of 17.1, 19.2, 28.4 and 30.4 (telescope T1, Ritchey–Chretien design) or 17.5 and 30.4 nm (telescope T2, Herschel telescope/coronagraphs, two channels with two detectors) [3]. The detector filters of these telescopes (Fig. 9a) were fabricated using identical, about 8.5-μm-thick track-etched PET membranes metallised on both sides and having 1.5-μm-diameter cylindrical through pores with a density of 1.4×10^7 cm^{-2}. Using a process developed by our group, 0.12-μm-thick aluminium films were produced on membranes with a formvar underlayer and then the formvar was removed from the free surface of the aluminium film. A filter on a porous substrate was placed with a small gap (about 0.7 mm) in front of the input MCP surface. In contrast to analogous filters made in the form of a porous membrane/thin film structure, which were used as detector filters in a previous flight of the CORONAS orbital station [30], here membranes with a high pore density and smaller pore diameter were used in order to improve the spatial resolution of the telescopes. Not only did this change ensured better resolution, but it also drastically reduced the transmittance of the filters for the long-wavelength background in the visible and near-IR spectral regions due to the diffraction filtering of radiation. Note that thin-film X-ray filters on track-etched membranes reliably operated on board the CORONAS-F station throughout its prolonged mission (about four years). The use of these filters helped to acquire rich experimental data for gaining insight into active processes in the Sun's corona by X-ray imaging spectroscopy techniques [4].

A word on the application of fine-structured filters in laser physics. For example, to produce quasi-monochromatic beams using a laser plasma source and spectral filtering in the wavelength range 10–14 nm, Kolachevsky et al. [28] fabricated and utilised a thin-film rhodium filter on a regular electroplated nickel grid with a 10-μm period (Fig. 1). A laser plasma was excited by frequency-doubled radiation from a Q-switched Nd:YAP laser at a wavelength of 0.54 μm. The filter fully intercepted the unwanted X-rays due to Fresnel reflection from a multilayer mirror and suppressed the visible and UV light from the plasma source.

In studies of the physical properties and metrology of laser plasma sources used in projection X-ray lithography, Bijkerk et al. [33, 34] and Shmaenok et al. [35] used thin-film molybdenum filters based on metallised track-etched membranes with micron diameter pores (Fig. 9b). Thin refractory metal films as free-standing films and X-ray filters are less common in experimental practice than are multilayer systems or aluminium films and foils. They are difficult to fabricate by existing techniques, especially if there are increased requirements for the mechanical strength of films. Our group's research and experiments helped to obviate this difficulty. As in the case of a filter with a silicon carbide film on a track-

etched membrane [30, 32], thin molybdenum and rhodium films on microstructured substrates with through holes were found to have good strength, with no disintegration during the fabrication process or in experiments, even though the deposits were stressed because of the large thermal expansion mismatch between the film and support structure materials. Not only did the small size of the through holes (and the small spacing between them) influence the thermal properties of the filters, but it also improved their mechanical properties and tensile strength, hindering the generation of cracks and other mechanical defects.

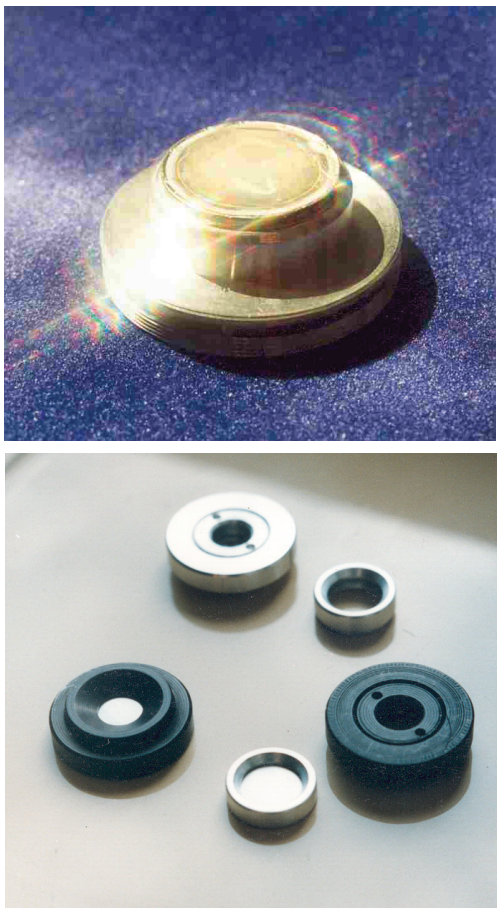

Figure 9. Photographs of filters on track-etched membranes in mounts: (a) aluminium filter for the MCP imaging detector in one of the channels of the telescope on board the CORONAS-F satellite [3, 4] and (b) molybdenum filters for laser emission diagnostics [33–35].

7. Conclusions

This paper addressed the fabrication of thin-film X-ray filters using microstructured substrates with through holes and standard methods for the sputter deposition of materials on a sample. Track-etched polymer membranes with through holes and metallic microgrids were used to produce samples of X-ray filters by direct sputter deposition on a substrate. The filters were subsequently used in solar X-ray telescopes fabricated at LPI and in laboratory instruments for laser plasma diagnostics. The use of massive fine-structured substrates was shown to help obviate many problems that are related to the heat dissipation, overheating and thermal breakdown of thin-film samples and arise in the fabrication of X-ray filters intended for application in the soft X-ray and vacuum UV spectral regions.

Acknowledgements. I recall with gratitude, warmth and esteem I.A. Zhitnik and I.I. Sobelman, our joint work and the creative atmosphere they maintained as heads of our research team and leaders in experimental X-ray astronomy at LPI. I am grateful to P.Yu. Apel, V.K. Bardin, F.A. Pudonin and their colleagues for the many years of cooperation and for their assistance in the fabrication of the filters. I thank A.V. Vinogradov, E.N. Ragozin and R.M. Feshchenko for their helpful comments regarding the manuscript. This work was supported by the RF Ministry of Education and Science (state research task No. 0023-0006).

References

1. Oraevskii V.N., Sobelman I.I., Zhitnik I.A., Kuznetsov V.D. *Usp. Fiz. Nauk*, **172**, 949 (2002).
2. Sobelman I.I., Zhitnik I.A., Val'nichek B., et al. Preprint FIAN No. 241 (Moscow: Fizicheskii Inst. im. P.N. Lebedeva Akad. Nauk SSSR, 1988) p. 18.
3. Zhitnik I., Kuzin S., Afanas'ev A., Bugaenko O., et al. *Adv. Space Res.*, **32** (4), 473 (2003).
4. Kuznetsov V.D. (Ed.) *The Coronas-F Space Mission: Key Results for Solar Terrestrial Physics* (Berlin: Springer, 2014; Moscow: Fizmatlit, 2009).
5. Seely J.F., Korde R., Hanser F., Wise J., Holland G.E., Weaver J., Rife J.C. *Proc. SPIE*, **3764**, 103 (1999).
6. Aruev P.N., Barysheva M.M., Ber B.Ya., Zabrodskaya N.V., Zabrodskii V.V., Lopatin A.Ya., Pestov A.E., Petrenko M.V., Polkovnikov V.N., Salashchenko N.N., Sukhanov V.L., Chkhalo N.I. *Quantum Electron.*, **42** (10), 943 (2012) [*Kvantovaya Elektron.*, **42** (10), 943 (2012)].
7. Hass G., Francombe M., Hoffman R. (Eds) *Physics of Thin Films: Advances in Research and Development* (New York: Academic, 1973; Moscow: Mir, 1977) Vol. 7.
8. Thompson B.J., Shannon R.R. (Eds) *Space Optics: Proc. 9th Int. Congress of the Int. Commission for Optics* (Washington, D.C.: National Academy of Sciences, 1974; Moscow: Mashinostroenie, 1980).
9. Mitrofanov A.V., Karban O.V., Sugonyako A., Lubomska M. *Poverkhnost*, **7**, 30 (2009).
10. Powell Forbes R., Vedde P.W., Lindblom J.F., Powell Stephen F. *Opt. Eng.*, **26** (9), 614 (1990).
11. Spiller E., Grebe K., Golub L. *Proc. SPIE*, **1160**, 66 (1989).
12. Powell Forbes R. *Proc. SPIE*, **1848**, 503 (1992).
13. Viitanen Veli-Pekka, Mutikainen Risto, Nenonen Seppo, Partanen Panu. *J. X-Ray Sci. Technol.*, **4**, 182 (1994).
14. Bogachev S.A., Chkhalo N.I., Kuzin S.V., Pariev D.E., Polkovnikov V.N., Salashchenko N.N., Shestov S.V., Zuev S.Y. *Appl. Opt.*, **55**, 2126 (2016).
15. Chkhalo N.I., Drozdov M.N., Kluenkov E.B., Kuzin S.V., Lopatin A.Ya., LuchinV.I., Salashchenko N.N., Tsybin N.N., Zuev S.Yu. *Appl. Opt.*, **55**, 4683 (2016).
16. Canfield L.R., Vest R., Woods T.N., Korde R. *Proc. SPIE*, **2282**, 31 (1994).
17. Roikh I.L., Koltunova L.N., Fedosov S.N. *Nanesenie zashchitnykh pokrytii v vakuume* (Vacuum Growth of Protective Coatings) (Moscow: Mashinostroenie, 1980) p. 21.
18. Godovskii Yu.K. *Teplofizika polimerov* (Thermophysics of Polymers) (Moscow: Khimiya, 1982) p. 73.
19. Ginzburg V.L. *Sbornik zadach po obshchemu kursu fiziki* (Problems in General Physics) (Moscow: Nauka, 1964).
20. Ludwig Reimer. *Transmission Electron Microscopy* (Springer series in Optical Sciences) (Berlin, Tokyo: Springer, 1997) Vol. 36, p. 468.
21. Yaroslavtsev A.B. (Ed.) *Membrany i membrannye tekhnologii* (Membranes and Membrane Technologies) (Moscow: Nauchnyi Mir, 2013) p. 126.

22. Kuptsov A.H., Zhizhin G.N. *Handbook of Fourier Transform Raman and Infrared Spectra of Polymers* (Amsterdam: Elsevier, 1998; Moscow: Tekhnosfera, 2013).
23. Fortescue P., Swinerd G., Stark J. (Eds) *Spacecraft Systems Engineering* (Chichester: Wiley, 2011; Moscow: Al'pina Pablisher, 2015).
24. Bramson M.A. *Infrared Radiation: A Handbook for Applications* (New York: Plenum, 1968; Moscow: Nauka, 1965).
25. Sala A. *Radiant Properties of Materials* (Amsterdam: Elsevier, 1986) p. 47.
26. Adamov D.B., Savinich V.S. *Inzh.-Fiz. Zh*., **37** (2), 285 (1979).
27. Gruner G. (Ed.). *Millimeter and Submillimeter Wave Spectroscopy of Solids* (Berlin, Heidelberg: Springer-Verlag, 1998) Vol. 74, p. 68.
28. Kolachevsky N.N., Kondratenko V.V., Mitropol'skii M.M., Mitrofanov A.V., Ragozin E.N., Fedorenko A.I., Yulin S.A. *Kratk. Soobshch. Fiz*., (3–4), 12 (1993).
29. *Trudy XXI Mezhdunarodn. simp. po nanofizike i nanofotonike* (Proc. Int. Symp. on Nanophysics and Nanophotonics) (Nizhnii Novgorod: NGU, 2017) Vol. 1, p. 408.
30. Mitrofanov A., Pudonin F., Starodubzev N., Zhitnik I. *Proc. SPIE*, **3406**, 35 (1998).
31. Mitrofanov A.V., Tokarchuk D.N. *Nucl. Instrum. Methods Phys. Res., Sect. A*, **282**, 546 (1989).
32. Mitrofanov A., Pudonin F., Zhitnik I. *Proc. SPIE*, **2280**, 272 (1994).
33. Bijkerk F., Shmaenok L., Louis E., van Honk A., van der Wiel M.J., Platonov Yu.A., Shevelko A.P., Mitrofanov A.V., Voβ F., Deso R., Frowein H., Nikolaus B. *Proc. SPIE*, **2015**, 128 (1993).
34. Bijkerk F., Shmaenok L., van Honk A., Bastiaensen R., Platonov Yu.A., Shevelko A.P., Mitrofanov A.V., Voβ F., Desor R., Frowein H., Nikolaus B. *J. Phys. III*, **4**, 1669 (1994).
35. Shmaenok L., Bijkerk F., Louis E., van Honk A., van der Wiel M.J., Platonov Yu., Shevelko A., Mitrofanov A., Frowein H., Nikolaus B., Voβ F., Desor R. *Microelectron. Eng*., **23**, 211 (1994).